LBL-37243
UC-414

Presented at the
7th European Symposium on Semiconductor Detectors
Schloss Elmau, Germany, May 7-10, 1995

P-TYPE SILICON DRIFT DETECTORS

J.T. Walton, B. Krieger, D. Krofcheck, R. O'Donnel,
G. Odyniec, M. Partlan, and N.W. Wang
Lawrence Berkeley National Laboratory
University of California, Berkeley, CA 94720

June 1995

This work was supported by the Director, Office of Energy Research, Division of Nuclear Physics of the Office of High Energy and Nuclear Physics of the U.S. Department of Energy under Contract DE-AC03-76SF00098

DISTRIBUTION OF THIS DOCUMENT IS UNLIMITED

recycled paper

DISCLAIMER

This report was prepared as an account of work sponsored by an agency of the United States Government. Neither the United States Government nor any agency thereof, nor any of their employees, make any warranty, express or implied, or assumes any legal liability or responsibility for the accuracy, completeness, or usefulness of any information, apparatus, product, or process disclosed, or represents that its use would not infringe privately owned rights. Reference herein to any specific commercial product, process, or service by trade name, trademark, manufacturer, or otherwise does not necessarily constitute or imply its endorsement, recommendation, or favoring by the United States Government or any agency thereof. The views and opinions of authors expressed herein do not necessarily state or reflect those of the United States Government or any agency thereof.

DISCLAIMER

Portions of this document may be illegible in electronic image products. Images are produced from the best available original document.

P-TYPE SILICON DRIFT DETECTORS

J.T. Walton, B. Krieger, D. Krofcheck, R. O'Donnell,
G. Odyniec, M.D. Partlan, N.W. Wang
Lawrence Berkeley National Laboratory, University of California,
Berkeley, CA, 94720, USA

ABSTRACT

Preliminary results on 16 cm^2, position-sensitive silicon drift detectors, fabricated for the first time on p-type silicon substrates, are presented. The detectors were designed, fabricated, and tested recently at LBL and show interesting properties which make them attractive for use in future physics experiments.

A pulse count rate of approximately $8x10^6$ s^{-1} is demonstrated by the p-type silicon drift detectors. This count rate estimate is derived by measuring simultaneous tracks produced by a laser and photolithographic mask collimator that generates double tracks separated by 50 μm to 1200 μm.

A new method of using ion-implanted polysilicon to produce precise valued bias resistors on the silicon drift detectors is also discussed.

This work was supported by the Director, Office of Energy Research, Division of Nuclear Physics of the Office of High Energy and Nuclear Physics of the U.S. Department of Energy under Contract DE-AC03-76SF0098.

I. INTRODUCTION

In recent years, position-sensitive silicon detectors have become indispensable in high energy physics experiments. However, the use of silicon strip detectors for tracking in high multiplicity environments is complicated by so-called ghost hits (ambiguities of combined one-dimensional information collected from multiple planes of strip detectors), and the use of silicon pixel detectors is expensive due to their large number of readout channels. An ideal detector for the high multiplicity collisions appears to be the silicon drift detector (SiDD) [1, 2]. Notable features of the silicon drift detector, besides its high position and energy resolution and very good two track resolution, include its small (~0.1 pF), area-independent output capacitance, modest readout electronics requirements, and minimal need for cooling.

In this paper, we describe our work on SiDDs which have been fabricated on p-type silicon rather than on the more typically used n-type silicon. We have investigated the use of p-type silicon as the starting material for SiDDs because of several benefits possibly to be gained. High purity, p-type silicon grown by the float-zone process exhibits better radial dopant uniformity than n-type, float-zone silicon. High purity, n-type silicon with the dopant uniformity required for position-sensitive SiDDs must be initially grown as very pure p-type material via the float-zone technique and subsequently neutron transmutation doped. Neutron transmutation doped silicon is expensive and available only by special order; float-zone, p-type silicon, on the other hand, is readily available and relatively inexpensive. In addition, float-zone silicon is free of the radiation damage caused by the neutron transmutation doping process; the response of neutron-induced defects to thermal annealing is complicated and can result in uncontrollable changes in material resistivity during detector processing [3]. Moreover, there has been some evidence recently that p-type silicon is more radiation-resistant than n-type [4]. In the following sections, we describe the structure of the p-type silicon drift detector (pSiDD), the characterization of its position resolution, and the development of ion-implanted polycrystalline silicon resistors for biasing the detector.

II. DEVICE DESCRIPTION

We fabricated the pSiDDs on 3" diameter, 300 μm thick, (111), 7 kΩ-cm, p-type, float-zone silicon. The process used to fabricate the detectors is described in detail elsewhere [5]. Figure 1 shows the structure of the position-sensitive pSiDD developed at LBL; the detector geometry was adapted from an n-type SiDD (nSiDD) designed by P. Rehak at

Brookhaven National Laboratory. In this work, the nomenclature of the n-type SiDDs has been retained, and thus we will refer to the n^+ contacts as "cathodes" and the p^+ contacts as "anodes." The pSiDD consists of 332 parallel cathodes formed on both sides of a p-type silicon substrate. The cathode pitch is 120 μm. At one end of the detector is a row of 178 anodes with 250 μm pitch. Around the active region is a high voltage guard region consisting of 30 μm wide n^+ strips. The guard structure is tapered so that there are more guard strips protecting the cathodes farther from the anodes (which will need to withstand higher voltages) than the cathodes nearer the anodes.

During detector operation, the cathodes are reverse biased to deplete the entire silicon substrate and to create a uniform electric field in the direction parallel to the surface. When electron-hole pairs are created by ionizing radiation passing through the detector, the electrons are quickly collected at the reverse biased cathodes. The holes, on the other hand, are focused down the center plane of the detector and drift at constant velocity toward the row of anodes at the low voltage end of the device. The transit time of the holes allows the distance of the incident radiation from the anode plane to be calculated. The distribution of the signal charge over the readout anodes gives the second position coordinate.

III. Detector Characterization

We have studied the performance of the pSiDDs using measurements of a) the drift time vs. position of the incident radiation (i.e., the linearity of the detector response), b) energy resolution, and c) single-track and double-track position resolution. In the following sections, we discuss the results of each type of measurement.

At this point, we would like to stress that the nSiDD and pSiDD should have identical position resolution capabilities. This comment is based on the assumption that the spatial growth of the signal charge packet (either electrons or holes) as it drifts down the detector is governed by diffusion. Based on this assumption, it is readily shown that, at room temperature, the rms spatial spread in the packet width, $\sigma(x)$, is given by

$$\sigma(x) = \sqrt{2\,Dt}$$

$$= \sqrt{\frac{2\,kT\mu}{q}\,\frac{X_o}{\mu\,E}}$$

$$\sigma(x) = 0.228\,\sqrt{\frac{X_o}{E}}\ \text{(cm)} \qquad (1)$$

where X_o is the distance (in cm) of the incident particle's point of interaction on the drift detector from the collecting anode, and E is the applied electric drift field (in V/cm), and is independent of any material properties. However, the speed with which the packet arrives at the collecting anodes is dependent on the carrier mobility, which is approximately three times less for holes than electrons. Therefore, if the drift detector signals were digitized at the anodes, the digitizing rate for the pSiDD could be about (μ_h/μ_e) times slower than for a nSiDD for the same number of sample points. Note also that the pSiDD peak amplitude would be (μ_h/μ_e) smaller than the nSiDD peak.

a) Drift time vs. Position

We have demonstrated that the pSiDDs collect signal charge across their entire 4 cm length, and that the drift time is a linear function of the incident position of the excitation [5]. Accurate measurements of the transit time as a function of the distance that the charge cloud drifts were achieved by attaching the detectors to a computer-controlled x-y stage that could be stepped in 0.5 μm increments. Infrared light (λ = 1.06 μm) from a pulsed Nd:YAG laser was focused through a microscope objective to a 5 μm diameter spot on the detector. Figure 2 shows the relation between the signal arrival time and laser position over a 7 mm distance, with an applied drift field of 263 V/cm. The relation is very linear, and its slope agrees with the expected drift velocity at this electric field to within 2%.

b) Energy Resolution

For energy resolution measurements, we placed an ^{241}Am source directly over the anode region and fed the charge signal through a hybrid preamplifier and a variable time constant amplifier to a multichannel analyzer. With a 0.25 μsec shaping amplifier time constant, we obtained an energy resolution of 3.04 keV FWHM at 59.4 keV. The ^{241}Am spectrum is shown in Figure 3. The noise contribution of the electronics alone, measured using a pulse generator input at the preamplifier, was 2.95 keV FWHM. This suggests that the pSiDDs can provide excellent energy measurement when equipped with lower noise electronics.

c) Single-Track and Double-Track Position Resolution

In our single-track and double-track measurements of the pSiDD performance we used the electronics described above. For determination of the system time resolution, which we used to assess the position resolution in the drift dimension, we added a time-to-amplitude converter (TAC) module. The TAC, when connected to the multichannel analyzer, allowed us to make the required system time resolution measurements.

i) Single-track resolution

To be able to determine the position of a 'hit' on a SiDD, two 'times' are needed - the 'time-zero' at which the particles hit the SiDD, t_o, which is typically provided by another detector in the system, and the time that the hit signal arrives at the SiDD anodes, t_s. The position, X_o, of the hit on the SiDD is then calculated from:

$$\begin{aligned} X_o &= (t_s - t_o)\, v_{drift} \\ &= (t_s - t_o)\, \mu E, \end{aligned} \tag{2}$$

where μ is the carrier mobility and E is the internal electric drift field. In the following we assume that any error in determining the position, X_o, is directly due to errors in determining t_s, or

$$\Delta X_o \sim \Delta t_s. \tag{3}$$

The rms system time resolution, Δt_S, is dependent on the signal level, V_S, the rms system noise, V_n, and shaping amplifier time constant, τ, as follows:

$$\Delta t_S \approx (V_n / V_S)\, 2\tau, \tag{4}$$

providing $V_n << V_S$, and $t_r << \tau$, where t_r is the input signal rise time. Since, at short shaping amplifier time constants,

$$V_n \sim \frac{1}{\sqrt{\tau}} \tag{5}$$

then

$$\Delta t_S \sim \sqrt{\tau} \tag{6}$$

Therefore, the single-track time resolution should improve slowly with decreasing amplifier time constants. As will be discussed, however, the SiDD anode signal itself presents a lower limit on τ.

We have summarized our system measurements in Table I as well as including an estimate of the limiting single-track position resolution based solely on system electronics performance. A few comments about Table I are required:

1. The system resolution measurements were obtained from the width of the 59.4 keV ^{241}Am peak.
2. The Δt_s calculated is obtained from Eq. 4 above and assumes a signal of 60 keV.
3. The position resolution is calculated for a pSiDD using the product of the hole mobility (480 cm^2/V-sec), the electric field (500 V/cm, the magnitude of the field used in these measurements) and the calculated time resolution.

Figure 4 shows a plot of the expected rms time variance, $\sigma(t)$, as a function of the detector length. The upper curve in Figure 4 is the calculated rms spatial broadening as a function of drift distance from the anodes; note that for a given distance the spatial broadening is identical for both electrons and holes. The lower two curves represent the calculated rms time spread as a function of drift distance from the anodes for n-type and p-type SiDDs; note that the time spread is different for electrons and holes by a factor of (μ_h/μ_e).

The spatial resolutions in Table I were calculated by neglecting that the signals from the SiDD anodes are Gaussian functions of time [6] and have a finite rise time. The anode signal rise time depends on the time variance as follows:

$$t_r \approx \sigma(t) \qquad (7)$$

The significant change in $\sigma(t)$ across the 4 cm long pSiDD does not permit, for optimum timing, the use of a fixed amplifier time constant. To obtain the optimum timing the amplifier time constant should be matched to the signal rise time, or

$$2\,\tau \approx \sigma(t) \qquad (8)$$

Comparison of the calculated spatial resolution in Table I with the expected spatial variance in Figure 4 shows that our electronics, when approximately matched to the expected anode signal rise time, does not contribute significantly to our measurements. We make use of this result in our estimates of double-track resolution in the following section.

ii) Double-track resolution measurements

To examine two-track resolution which is not affected by the position dependence of time variance, we have chosen to measure it over a limited distance near the collecting anodes. The results presented here are included to show the potential of the pSiDDs and

the technique we have used, and not to provide a definitive answer on the double-track resolution capabilities of the pSiDDs.

In making the double-track resolution measurements one needs to keep in mind that the charge sensitive preamplifier used imposes certain limitations, namely that it integrates the Gaussian signal from the pSiDD anodes. Figures 5a &b show two simulated Gaussian pulses separated by 3σ and 4σ, respectively. The dashed line represents the integral of the Gaussians. This demonstrates that a separation of more than 3σ is needed for the charge sensitive preamplifier to resolve two peaks without further signal processing techniques.

Our experimental arrangement for making the double track measurements is shown in the insert of Figure 6. The glass plate in the figure is a chrome photolithography mask on which a pattern of 5 μm x 100 μm holes was etched. The photomask is aligned to the detector such that the 100 μm hole dimension is parallel to the pSiDD cathode stripes; the photomask can be placed directly on the detector, pattern side down, since the mask is made of insulating chrome oxide. The laser is defocused to spread light over several of the pinholes in the opaque chrome, in order to simulate multiple simultaneous tracks through the pSiDD. The intensity of the laser was adjusted to generate charge signals approximately equivalent to those deposited by minimum ionizing particles.

Results of this measurement are shown in Figure 6. The shaping amplifier time constant used in these measurements was 20 ns. Four distinct peaks can be seen, corresponding to signals coming through seven pinholes in the mask. The holes are spaced at intervals of 50, 100, 150, 300, 600 and 1200 μm. The peaks centered at 336 ns, 568 ns, and 1053 ns are due to light entering through single holes. The feature centered at 148 ns represents a superposition of signals from the four holes spaced 50, 100, and 150 μm away from each other. Thus, the smallest separation between two pinholes which could be resolved was 300 μm. The placement of the chrome mask on the detector (at about 4 mm from the anodes) was such that the time spread, $\sigma(t)$, was ~40 ns.

As seen in Figure 5, the holes in the plate must be more than 3 $\sigma(t)$ (120 ns or 300 μm) apart in order to be resolved by these electronics. Therefore, the results at small pinhole spacings in Figure 6 are consistent the discussion above.

The solid line in Figure 6 shows a fit of four Gaussians to the data. The width of the Gaussians is 65 ns. As shown in Table II, the fitted centroids of the signals match the time separations calculated from the known spacings between the pinholes very well. This result confirms our estimates in Table I that our electronics system noise would not influence the double-track measurements.

IV. DEVELOPMENT OF POLY-SI VOLTAGE DIVIDER

We have developed a process for fabricating a polycrystalline silicon (poly-Si) voltage divider on the pSiDDs. Since the position resolution of the SiDD depends on maintaining a constant carrier drift velocity and thus a constant drift field, the voltage divider resistors must be uniform. There have been several approaches to integrating bias resistors on silicon drift detectors. The Brookhaven n-type SiDD design used lightly ion implanted regions at the edges of the cathodes to make a resistor chain on the detector [7]. Other resistor integration schemes [8,9] have utilized the repeating MOSFET-like structure of the cathodes by depositing a metal gate over the SiO_2 region separating the cathodes.

The poly-Si approach has several advantages over the techniques mentioned above: e.g., poly-Si can better withstand high voltages than lightly implanted silicon resistors which are likely to exhibit punchthrough, and poly-Si resistors are neither voltage-dependent nor constrained within a small range of operating voltages, as they are with the MOS voltage dividers. Furthermore, it was believed that poly-Si would yield better uniformity of resistances than the other techniques, due to the good thickness control attainable with the low pressure chemical vapor deposition method used. Poly-Si resistors have been used for integrated circuits [10,11] and silicon strip detectors.

The resistivity of poly-Si can be varied between $\sim 10^6$ and $\sim 10^{-3}$ Ω-cm by varying dopant concentration [12], and thus easily allows fabrication of resistors within our target range of 200-300 kΩ. This range of resistance values was determined by compromising between the need for a high resistance value to limit power dissipation and the need for a lower resistance value so that small fluctuations in resistor current do not lead to large voltage fluctuations. A main concern in designing the fabrication process to yield precise-valued resistors was that the resistivity of poly-Si varies very rapidly with dopant concentration, so that small fluctuations in dopant concentration would result in large variations in resistor values. For this reason, ion implantation was chosen as the doping method, since it allows good control over dopant concentration and uniformity.

The proposed structure of the poly-Si resistor network, as it will be incorporated on to the pSiDD, is shown in Figure 7. Low temperature chemical vapor deposition is used to deposit a SiO_2 spacer layer over the detector after the n^+ and p^+ regions have been patterned and to deposit an undoped amorphous Si layer over the SiO_2. The amorphous Si layer is ion implanted with phosphorus and then annealed to activate the dopants and to yield polycrystalline microstructure. The resistors are then patterned and etched. Contacts between the resistors and cathodes are formed by etching windows in the low temperature

SiO_2 layer and depositing and patterning Al contacts. Resistors fabricated using this process have been tested alone but not as yet integrated on to the detectors.

To determine the phosphorus implant dose, we fabricated resistors using four different implant levels. The sheet resistance vs. implant dose is shown in Figure 8. The data indicate that the sheet resistance varies less rapidly at higher doses, which means that, for higher doses, local fluctuations in implant dose will have less effect on resistance. The resistors fabricated using this technique were quite uniform; the measured variation in sheet resistance over an 8 cm^2 area was $\pm 2\%$ at 1×10^{14} cm^{-2} and $\pm 1\%$ at 1×10^{15} cm^{-2}.

V. CONCLUSIONS

We have highlighted some of our recent research and development on p-type silicon drift detectors. In particular, we have demonstrated a novel technique for measuring the double-track resolution capabilities of these detectors and have also shown results on a possible technique for fabricating the precise, high-valued resistors needed for biasing the detectors.

Using "off-the-shelf" electronics we have been able to resolve double tracks separated by about 300 μm on the detector, which corresponds to a count rate of about 8 MHz. As noted in the paper, this rate was limited by our use of a charge sensitive preamplifier, not by the p-type silicon drift detector itself.

The excellent resistor uniformity from the ion-implanted polysilicon process described should allow creation of more uniform drift electric fields than we have presently been able to realize. Using the double-track measurement capability that we have developed, we expect shortly to confirm the viability of the polysilicon resistor approach.

ACKNOWLEDGMENTS

We thank P. Rehak of Brookhaven National Laboratory for allowing us access to his detector mask designs, and S.E. Holland of Lawrence Berkeley Laboratory for his advice on polysilicon resistor fabrication.

FIGURE CAPTIONS

Figure 1. Schematics showing a) cross-sectional view, and b) top view of the pSiDD.

Figure 2. Drift time versus position of the incident laser pulse.

Figure 3. ^{241}Am spectrum measured with the pSiDD. The energy deposited by the 59.4 keV gamma-ray is about 2/3 that of a minimum ionizing particle passing through 300 μm of silicon.

Figure 4. The calculated rms spatial broadening (top curve) and the calculated rms time spread (lower two curves) as a function of drift distance from the anodes. The spatial broadening is identical for both n-type and p-type SiDDS, whereas the spread in time is different by a factor of (μ_h/μ_e). An electric field of 500 V/cm was assumed for the calculations. This figure is similar to that of Fig. 10 in Ref. [6].

Figure 5. Simulated Gaussian pulses separated by 3σ and 4σ. The dashed line represents the integral of the Gaussians. This illustrates that a separation of more than 3σ is needed for the charge sensitive preamplifier to resolve two peaks without further signal processing techniques.

Figure 6. Signals measured by using a Cr photomask to collimate infrared light for simulating multiple tracks in the pSiDD. The insert shows a schematic of the technique. The laser is defocused to illuminate an array of 5 μm x 100 μm holes spaced at intervals of 50, 100, 150, 300, 600 and 1200 μm. The measured peaks centered at 336 ns, 568 ns, and 1053 ns are due to light entering through single holes. The feature centered at 148 ns represents a superposition of signals from four holes. The amplifier shaping time was 20 ns.

Figure 7. Schematics of a) top view and b) cross section of the poly-Si resistors as they will be integrated on the pSiDDs.

Figure 8. Measurements of sheet resistance vs. phosphorus implant dose. The variation in sheet resistance over an 8 cm^2 area was ±2% at 1x10^{14} cm^{-2} and ±1% at 1x10^{15} cm^{-2}.

Table I

Single-Track Timing and Position Resolution

Amplifier Time Constant	System FWHM measured	Δt_s rms calculated	Δt_s rms measured	Position resolution, rms, calculated
100 ns	4.3 keV	4.2 ns	2.0 ns	10.5 μm
50 ns	6.0 keV	3.2 ns	1.6 ns	8.0 μm
20 ns	9.6 keV	1.9 ns	1.2 ns	4.7 μm

Table II

Comparison of Times Between Signals (from Gaussian Fit) and Time Calculated from Pinhole Spacing

Pinhole spacing	475 μm *	600 μm	1200 μm
Calculated time separation	190 ns *	240 ns	480 ns
Measured time separation	188 ns	232 ns	485 ns

*Note: The spacing was averaged over the pinholes that appear in this peak. Based on this average spacing the time was calculated using a hole mobility of 500 $cm^2/V\text{-}s$ and and electric field of 500 V/cm.

REFERENCES

[1] E. Gatti and P. Rehak, Nucl. Instr. and Meth. 225 (1984) 608.

[2] E. Gatti, P. Rehak, and J.T. Walton, Nucl. Instr. and Meth. 226 (1984) 129.

[3] J.C. Corelli and J.W. Corbett, "Impact of Defects Formed in Neutron Transmutation Doping of Silicon on Device Performance," in *Neutron Transmutation Doped Silicon*, ed. J. Guldberg (Plenum Press, 1981) p. 35.

[4] E. Beuville et al., Nucl. Instr. and Meth. A288 (1990) 68.

[5] N.W. Wang et al., IEEE Trans. Nucl. Sci., to be published.

[6] E. Gatti, A. Longoni, P. Rehak, M. Sampietro, Nucl. Instr. and Meth. A253 (1987) 393.

[7] W. Chen, H.W. Kraner, Z. Li and P. Rehak, IEEE Trans. Nucl. Sci. 41 (1994) 941.

[8] A. Bischoff et al., Nucl. Instr. and Meth. A326 (1993) 27.

[9] P. Lechner et al., Proc. of the 6th European Symposium on Semiconductor Detectors, Milan, February 1992, MPI-PhE/92-12.

[10] N. Lu, L. Gerzberg, C. Y. Lu., and J. D. Meindl, IEEE Trans. Elec. Dev. ED-28 (1981) 812.

[11] T. Ohzone et al., IEEE Trans. Elec. Dev. ED-32 (1985) 1749.

[12] T.I. Kamins, *Polycrystalline Silicon for Integrated Circuit Applications* (Kluwer Academic Press, 1988).

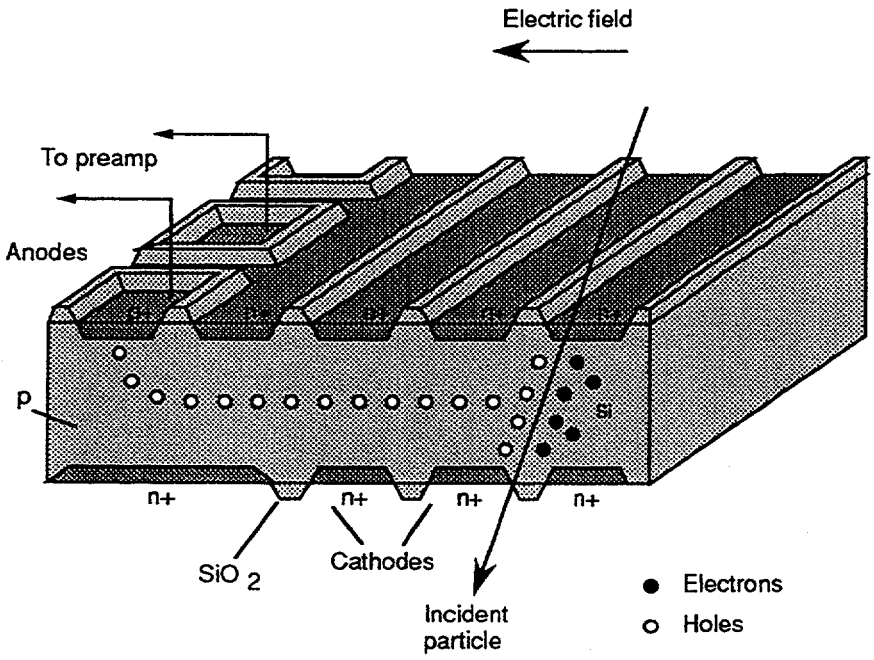
Electric field
To preamp
Anodes
p
n+
n+
n+
n+
Si
SiO 2
Cathodes
Incident
particle
Electrons
Holes

Figure 1a.

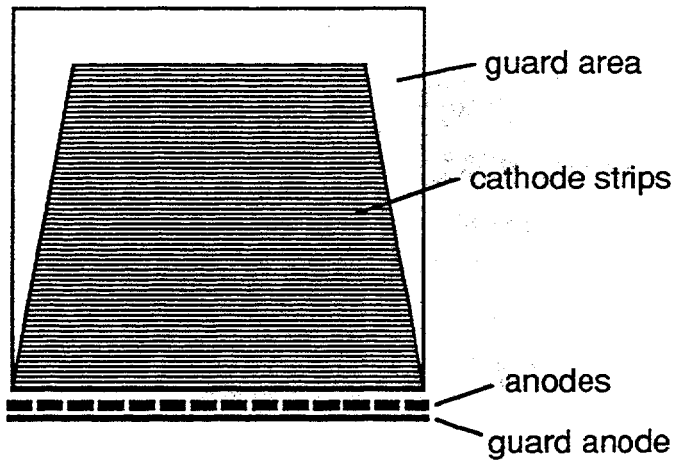

Figure 1b.

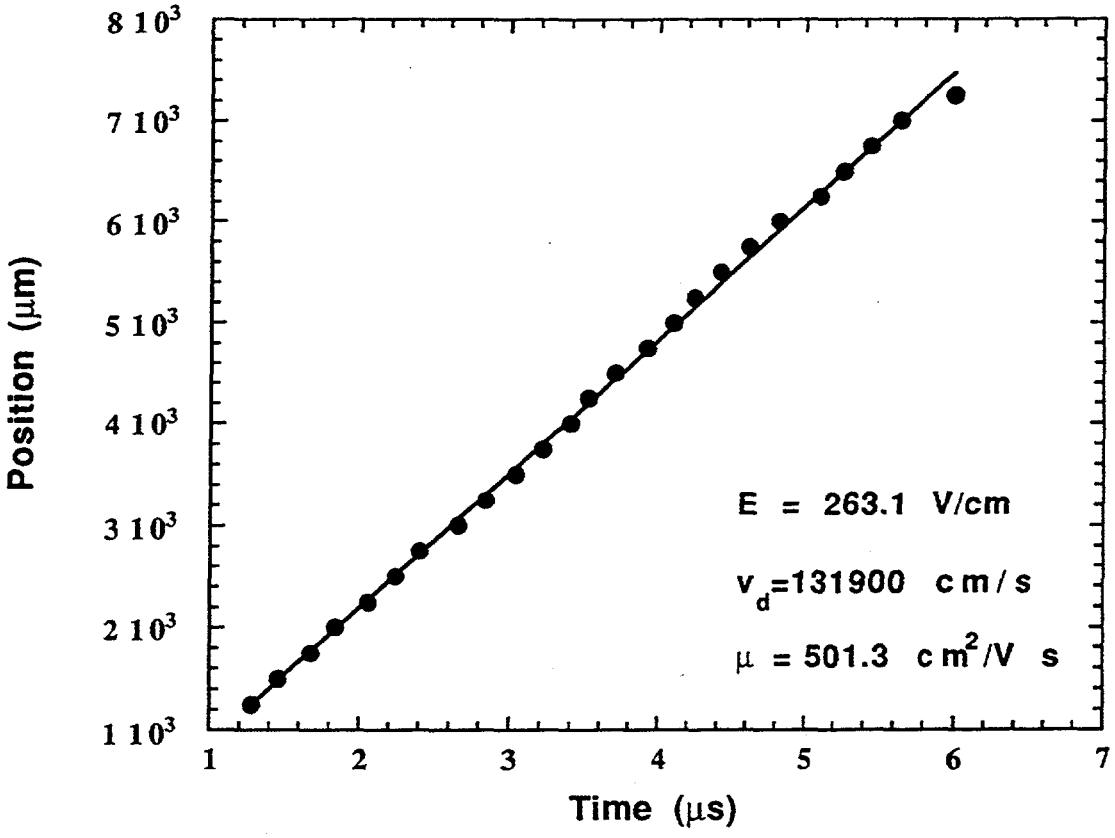
8 10³
7 10³
6 10³
5 10³
4 10³
3 10³
2 10³
1 10³
Position (μm)
1
2
3
4
5
6
7
Time (μs)
E = 263.1 V/cm
v_d=131900 cm/s
μ = 501.3 cm²/V s

Figure 2

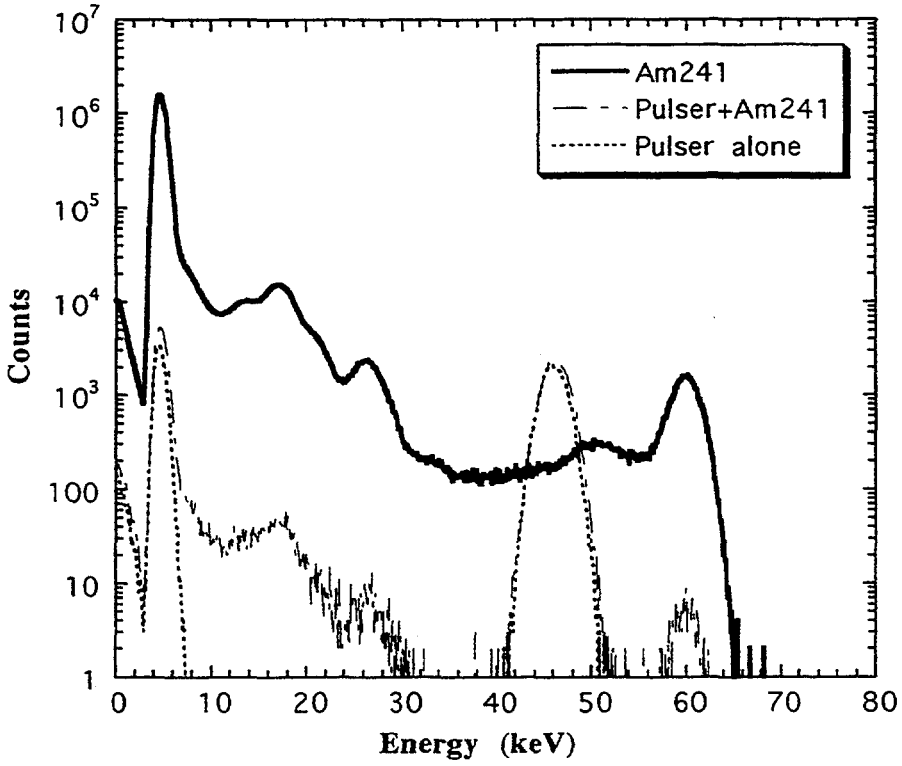
Am241
Pulser+Am241
Pulser alone
Counts
Energy (keV)
10^7
10^6
10^5
10^4
10^3
100
10
1
0
10
20
30
40
50
60
70
80

Figure 3

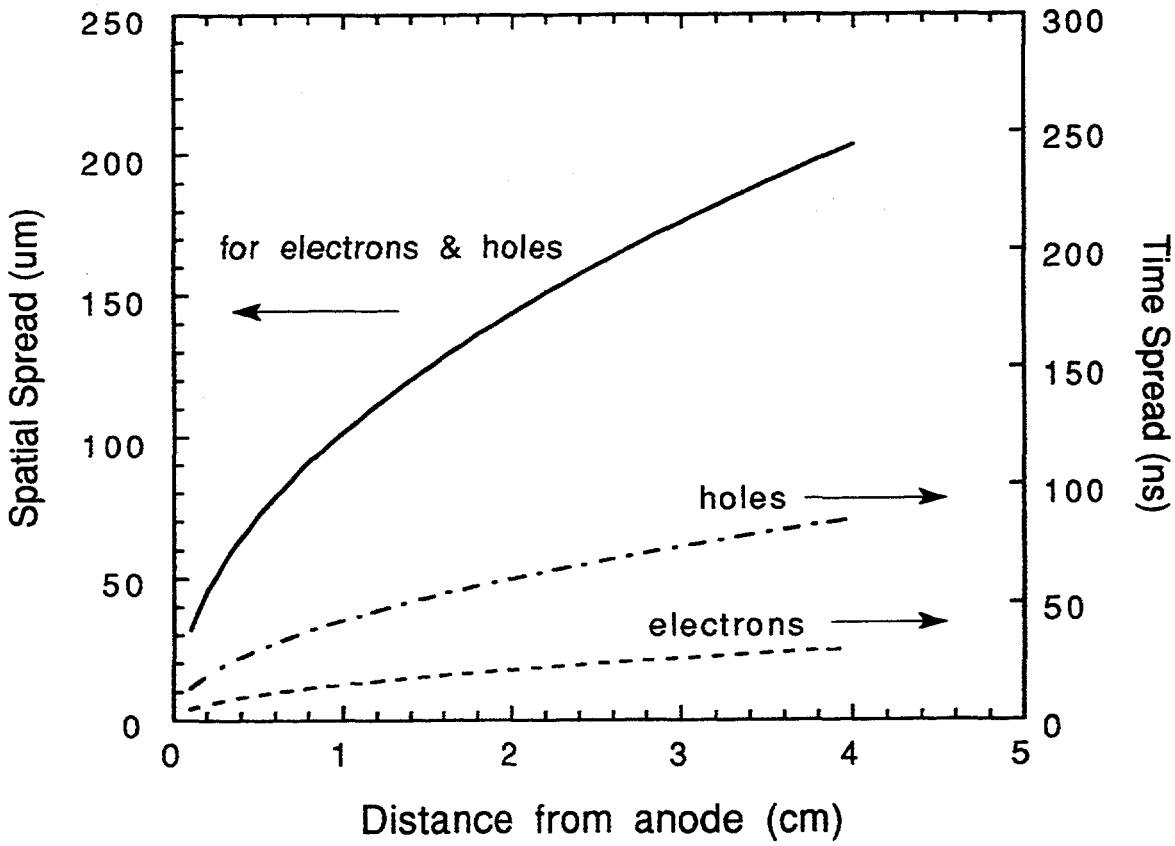
250
200
150
100
50
0
Spatial Spread (um)
for electrons & holes
holes
electrons
300
250
200
150
100
50
0
Time Spread (ns)
0
1
2
3
4
5
Distance from anode (cm)

Figure 4

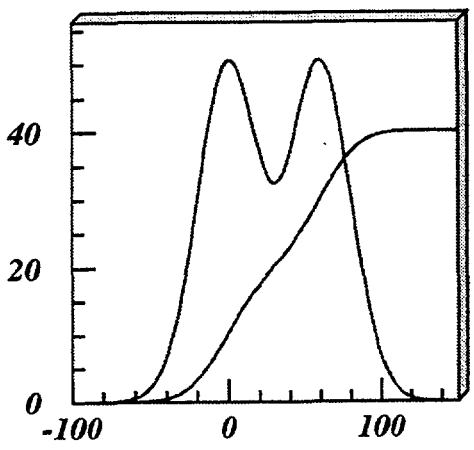

Figure 5a.

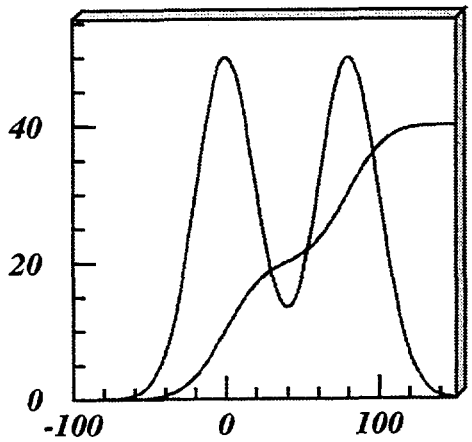

Figure 5b.

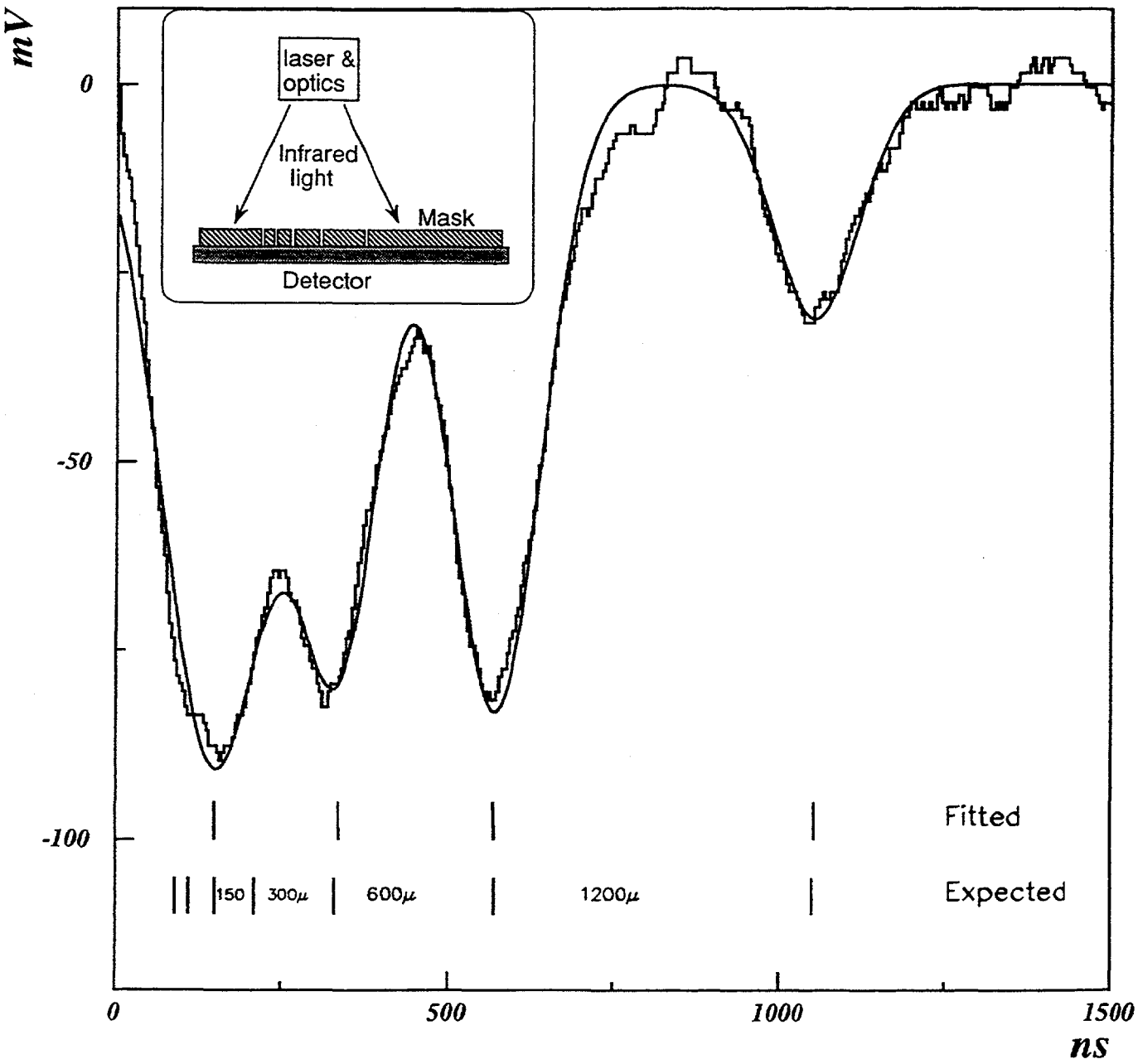
mV
0
-50
-100
laser &
optics
Infrared
light
Mask
Detector
Fitted
Expected
150
300μ
600μ
1200μ
0
500
1000
1500
ns

Figure 6

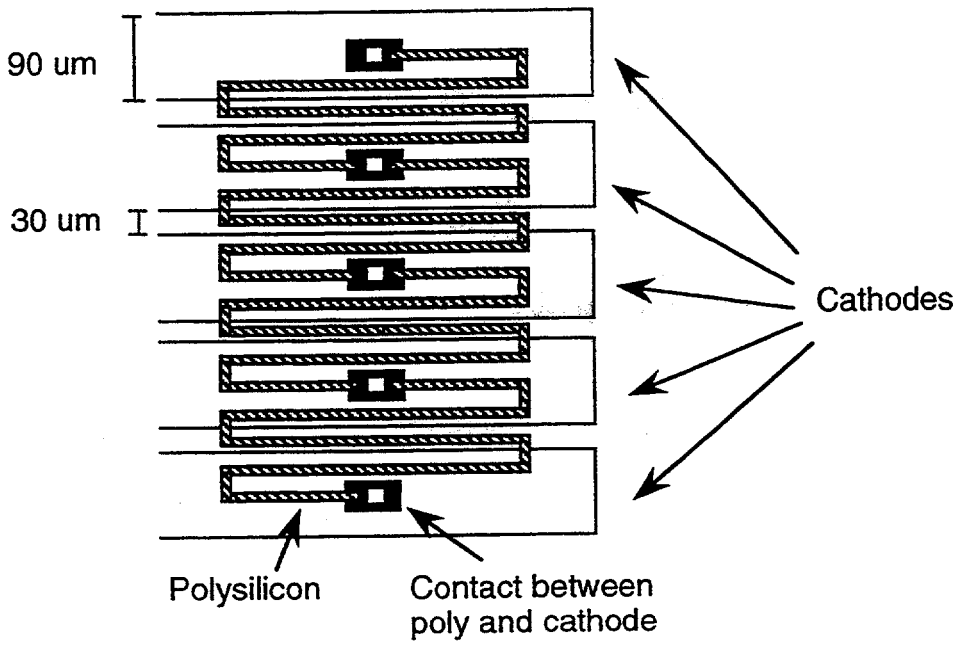
90 um
30 um
Cathodes
Polysilicon
Contact between
poly and cathode

Figure 7a.

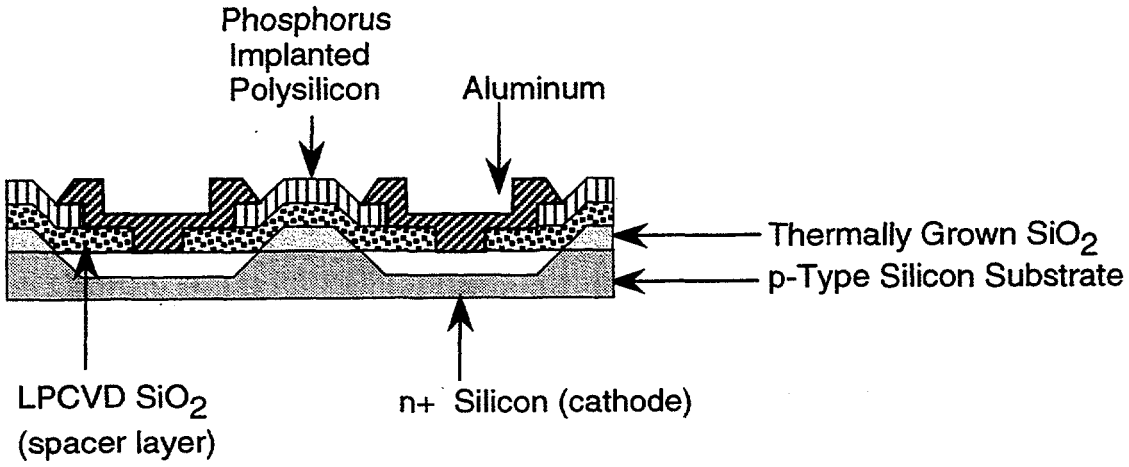
Phosphorus
Implanted
Polysilicon
Aluminum
Thermally Grown SiO_2
p-Type Silicon Substrate
LPCVD SiO_2
(spacer layer)
n+ Silicon (cathode)

Figure 7b.

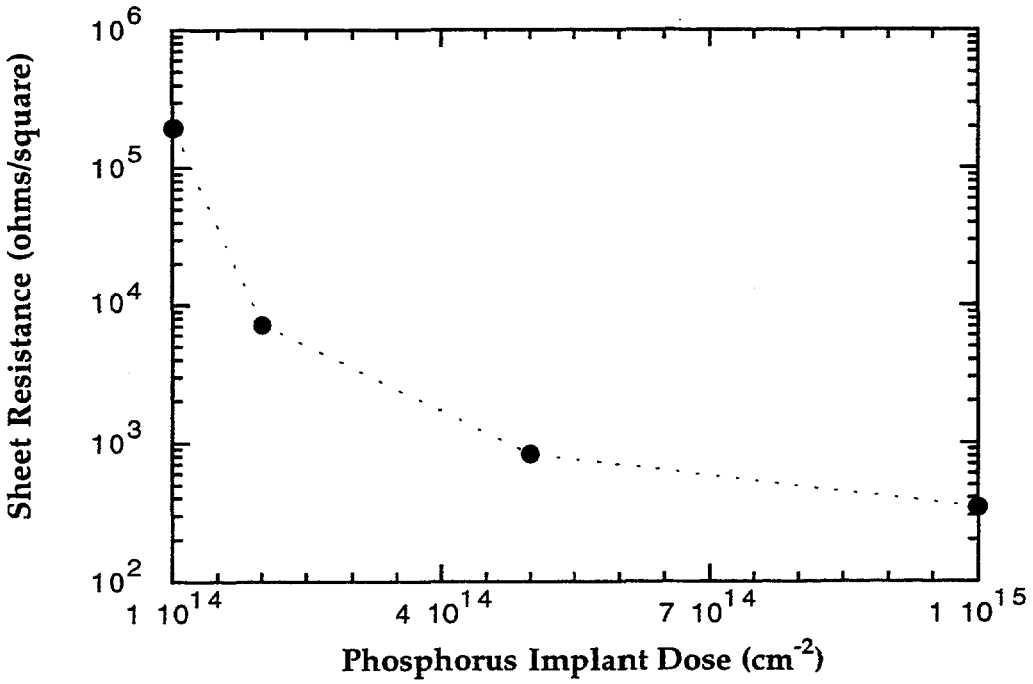
Sheet Resistance (ohms/square)
10^6
10^5
10^4
10^3
10^2
1 10^14
4 10^14
7 10^14
1 10^15
Phosphorus Implant Dose (cm^-2)

Figure 8